Climate Dynamics (2002) 19: 343–353
DOI 10.1007/s00382-002-0231-2

Y. Tang · W.W. Hsieh

Hybrid coupled models of the tropical Pacific: II ENSO prediction

Received: 20 August 2001 / Accepted: 11 January 2002 / Published online: 7 June 2002

Abstract Two hybrid coupled models (HCMs), a dynamical ocean model coupled to a nonlinear neural network atmosphere (NHCM), and the same ocean model coupled to a linear regression atmosphere (LHCM), are used to investigate ENSO (El Niño-Southern Oscillation) prediction skills, and to test whether having a nonlinear empirical atmospheric model leads to improvements over HCMs with only a linear atmosphere. Predictions of sea surface temperature anomalies (SSTA) and sea level height anomalies (SLHA) show that (1) although both coupled models can fairly well predict the SSTA and SLHA variations in the equatorial eastern Pacific at lead times of 1 year or so, the LHCM displayed less consistent skills than the NHCM over the decades, with considerably lower skills in the 1990s; (2) both models have better correlation skills in the SLHA predictions than in SSTA predictions for all lead times; and (3) the regions of high correlation skills shifted eastward in the 1990s. A nonlinear canonical correlation analysis of the zonal wind stress anomalies and the SSTA shows that their relation was indeed more nonlinear in the 1990s than in the 1980s, which would give the NHCM an advantage over the LHCM in the 1990s.

1 Introduction

Models for ENSO prediction can be categorized into purely statistical models, hybrid coupled models and coupled ocean–atmosphere models. Statistical models have several drawbacks as discussed in Latif et al. (1998): (1) forecast skills degrade relatively quickly with increasing lead time; (2) artificial skill remains a problem in all statistical forecast schemes; and (3) a statistical relationship does not always imply a causal relationship.

In coupled ocean–atmosphere models, the forecast skills drop more slowly with increasing lead time than in the statistical models. The problems associated with the coupled models are: (1) climate drift exists in almost all CGCMs (coupled general circulation models); (2) some physical processes still have to be parameterized; (3) proper initialization of the coupled model is difficult; and (4) the cost is very much greater than statistical models.

The hybrid-coupled model (HCM) combines a dynamical ocean model with a statistical atmospheric model for coupled interaction studies (Barnett et al. 1993; Syu and Neelin 2000; Balmaseda et al. 1994). HCM shares the advantages of both dynamical models and statistical models, although some drawbacks associated with the dynamical model and statistical model are also retained. The main advantages of a hybrid model are: (1) the climate drift problem is avoided, (2) easier understanding of the coupled mechanisms and lower computing cost than a full CGCM (Blanke et al. 1997), and (3) comparable or even better simulation and prediction skills relative to a CGCM (Palmer and Anderson 1994; Kang and Kug 2000).

Currently, all empirical atmospheric models used in HCMs have been linear statistical models. Although the dynamic response of the atmosphere and ocean in the tropical Pacific is quasi-linear (Tang et al. 2000; Tang et al. 2001), the coupled interactions between the two components seem more complicated than the relations extracted from data and from uncoupled model responses. In part I of this study (Tang 2002), two HCMs of the tropical Pacific were studied for their interannual variability. The first, the 'linear' hybrid coupled model (LHCM) has a six-layer nonlinear dynamical ocean

Y. Tang (✉) · W.W. Hsieh
Department of Earth and Ocean Sciences,
University of British Columbia,
Vancouver, BC, Canada
E-mail: ytang@cims.nyu.edu

Present address: Y. Tang
CAOS, Courant Institute of Mathematical Sciences, New York University, 251 Mercer Street, New York, NY 10012, USA

model coupled to a linear regression atmospheric model. The second, the 'nonlinear' HCM (NHCM) has the same ocean model but a nonlinear neural network atmospheric model. The results show that the NHCM can produce more realistic ENSO oscillatory behavior, with a period of about 57 months in comparison with a period of 87 months in the LHCM. In this part II, we study the differences between the NHCM and LHCM in ENSO prediction. Section 2 briefly describes the prediction models. Section 3 displays the prediction skills for SSTA and SLHA. Section 4 analyses the decadal differences of prediction skills by NLCCA. A summary is given in Sect. 5.

2 Model description

The ocean and atmospheric models used in this study are almost identical to those in Tang et al. (2001), and in Part I of this study (Tang 2002). The ocean model consists of a tropical Pacific model with six active layers allowing for an exchange of mass, momentum and heat at each layer interface by a parameterization of entrainment, with a horizontal resolution of $1.5° \times 1.5°$, covering the area 30°N–30°S in latitude and from 123°E–69°W. The time step is two hours. The atmospheric model is a statistical model using either linear regression (LR) or neural network (NN) (Hsieh and Tang 1998) to reconstruct the atmospheric wind stress using ocean states as predictors. Further details of the ocean model and the construction of linear and nonlinear atmospheric models can be found in Tang et al. (2001) and Tang (2002).

For both NHCM and LHCM, two kinds of prediction experiments were carried out in this study, 'hindcasts' from 1964–1990 and 'forecasts' from 1990–1998. More precisely, during the 'forecast' period, the latest forecasts were made in 1998, but the forecasts actually extended into 1999, while during the 'hindcast' period, the forecasts extended into 1991. To alleviate the artificial skills, the cross-validated atmospheric models described in Tang et al. (2001) were used in the hindcasts experiments, i.e., the atmospheric models were developed excluding data from the hindcast period. For example, when the period 1970–1980 is being hindcasted, the atmospheric models used were only built from the data of 1964–1969 and 1981–1990. Thus, no data from the hindcast period have entered the coupled model through LR or NN reconstructed winds in any hindcast experiments. For the forecast experiments of 1990–1998, the atmospheric models are the ensemble of individual cross-validated models built for the hindcast experiments from 1964–1990, so data from 1990–1999 were never used in model building. There is a slight difference with the atmospheric models used in Part I of this study (Tang 2002) where the atmospheric models were built using data from the whole period of 1964–1990. In addition, the atmosphere models with upper ocean heat content as predictors were used here for all the prediction experiments because they yield slightly better skills than the atmospheric models with SST as predictors (Tang et al. 2001). The dynamical behavior and interannual variability of the coupled models with cross-validated atmospheric models and with upper ocean heat contents as predictors are generally very similar to these described in Part I (Tang 2002).

An important factor affecting the ENSO oscillation and model predictability is the coupling coefficient δ (Tang 2001), as the change in the coupling strength can easily modify the amplitude of the coupled oscillation, and exert a strong influence on the frequency locking behavior (Chang et al. 1996; Tang 2002). After many sensitivity experiments, we found that the best hindcast and forecast skills for LHCM and NHCM are not attained either from the standard coupling with regular ENSO oscillations as in Part I (Tang 2002), or from stronger coupling than the standard coupling. The best hindcast and forecast skills occurred for 'damped' coupling, with δ between 0.7 to 0.8. We thus chose δ to be 0.7 for all hindcast and forecast experiments presented in this study for both NHCM and LHCM. The seasonal cycle, used to obtain the surface sea temperature anomalies (SSTA) for evaluating the model skills, was calculated from the hindcast experiments during 1964–1990.

3 ENSO predictions

The ocean model was forced with the observed FSU (Florida State University) wind stress (Goldenberg and O'Brien 1981) from 1961 to 1998. From April, 1964 onward, at three month intervals (1 January, 1 April, 1 July, 1 October), the conditions of this control run were selected as the initial conditions for the NHCM and LHCM, which were run for 15 months. For each HCM, a total of 104 runs were made starting from April 1964 to January 1990 (the hindcast period), and 35 runs starting from April 1990 to October 1998 (the forecast period). Two physical variables, SSTA and SLHA, are used to examine the model's ENSO prediction skills.

3.1 SSTA prediction

Figures 1 and 2 show the correlation and RMSE (root mean square error) skills of the predicted tropical Pacific SSTA by the NHCM, for the hindcast period and the forecast period. The correlation skills (Fig. 1) are manifested mainly in the central and eastern equatorial Pacific like other ENSO models (e.g., Barnett et al. 1993; Chen et al. 1997), decreasing toward the west and higher latitudes, and with the lead time. The maximum RMSE resides in the equatorial eastern Pacific (Fig. 2), associated with the high skewness and variance in the region.

Comparing the prediction skills between the hindcast and forecast period, we noted several differences: (1) the good correlation skills during the hindcast period of 1964–1990 are centered further west of these during the forecast period of 1990–1998; (2) the RMSE is lower during the hindcast period than during the forecast period; (3) for the forecast period, besides high RMSE along the east coast, there is a high RMSE area centered around 150°W which is absent during the hindcast period. These differences are also manifested in the prediction skills of the LHCM (Fig. 3).

There are two possible reasons why the prediction skills have rather different features between the hindcast period and the forecast period. The first is due to the construction of the atmospheric models where the hindcast period was associated with the model training process whereas the forecast period is completely independent of training. However, we tested the other NN and LR empirical models built with the observational data of 1964–1998, which still manifested the differences of prediction skills between the two periods. Thus the second reason, i.e., the decadal variability in Pacific ocean leads to the differences in the prediction skills between the two periods, appears to be true.

Decadal dependence of ENSO predictability has been found in many ENSO forecast models (e.g., Balmaseda et al. 1995; Chen et al. 1997; Flügel and Chang 1998). While all models tended to have very good forecast skills in the 1980s, they suffered low skills in the 1990s, even with an improved initialization strategy (Chen et al. 1997). A clear contrast in terms of the characteristics of the interannual variability between the 1980s and the 1990s also exists in many observations such as sea level pressure, SST, low-level zonal wind, and subsurface ocean heat content anomalies in the Pacific (Kleeman et al. 1996; Latif et al. 1997; Ji et al. 1996). It has been suggested that the mechanism of decadal dependence of predictability is associated with the decadal changes in the mean state leading to decadal variability of ENSO (e.g., Wang 1995; Zhang et al. 1997). Several recent studies suggested that the changes in mean state is probably caused by (1) the remote response in the tropical atmosphere to the mid-latitude decadal oscillations

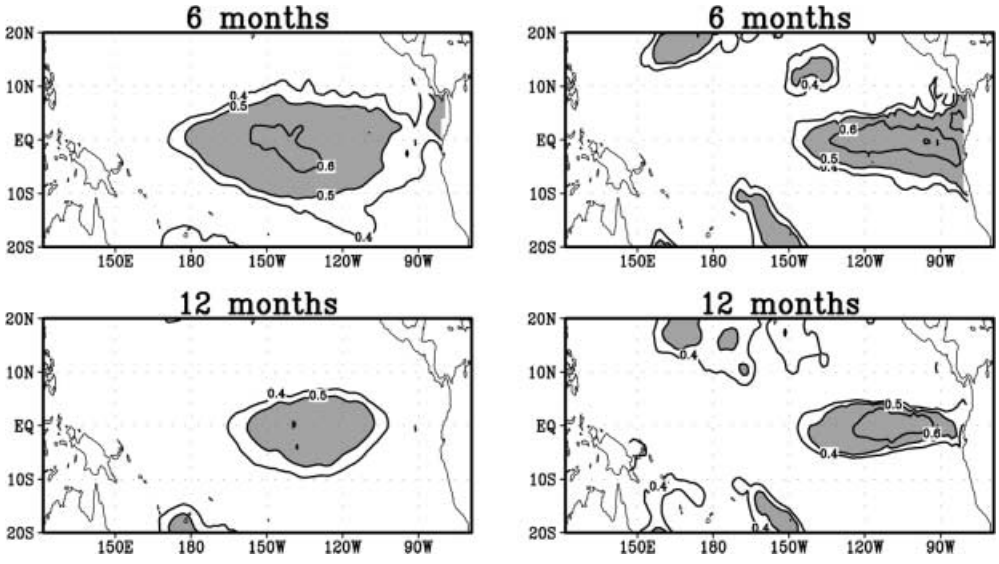

Fig. 1. Correlation skills for the predictions of SST anomalies in the tropical Pacific for the hindcast period from 1964–1990 (*left panels*), and the forecast period from 1990–1998 (*right panels*), by the NHCM for lead times of 6 and 12 months. Contour interval = 0.1 and positive values over 0.5 are *shaded*

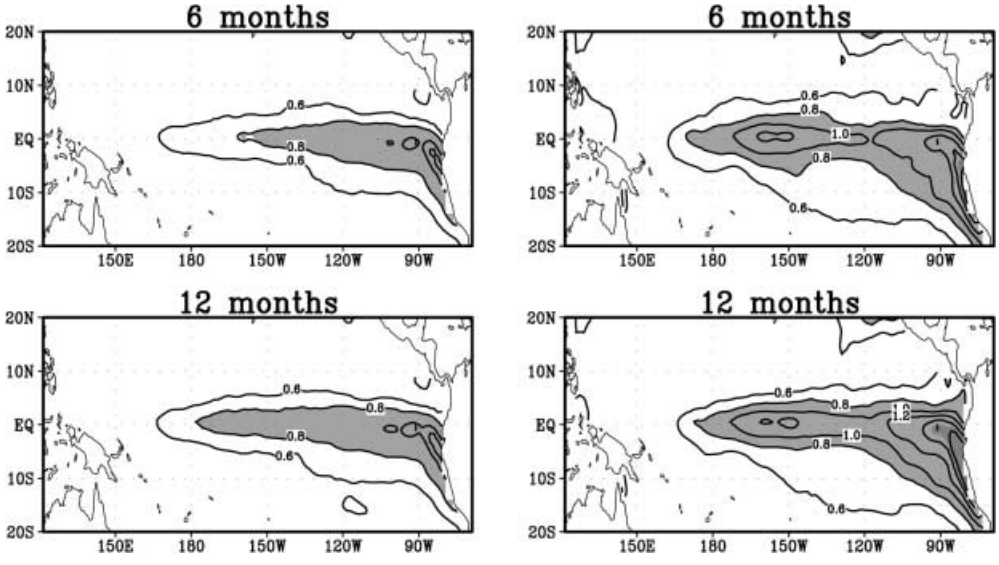

Fig. 2. RMSE skills for the predictions of SST anomalies in the tropical Pacific for the hindcast period from 1964–1990 (*left panels*), and the forecast period from 1990–1998 (*right panels*), by the NHCM. Contour interval = 0.2 °C and positive values over 0.8 °C are *shaded*

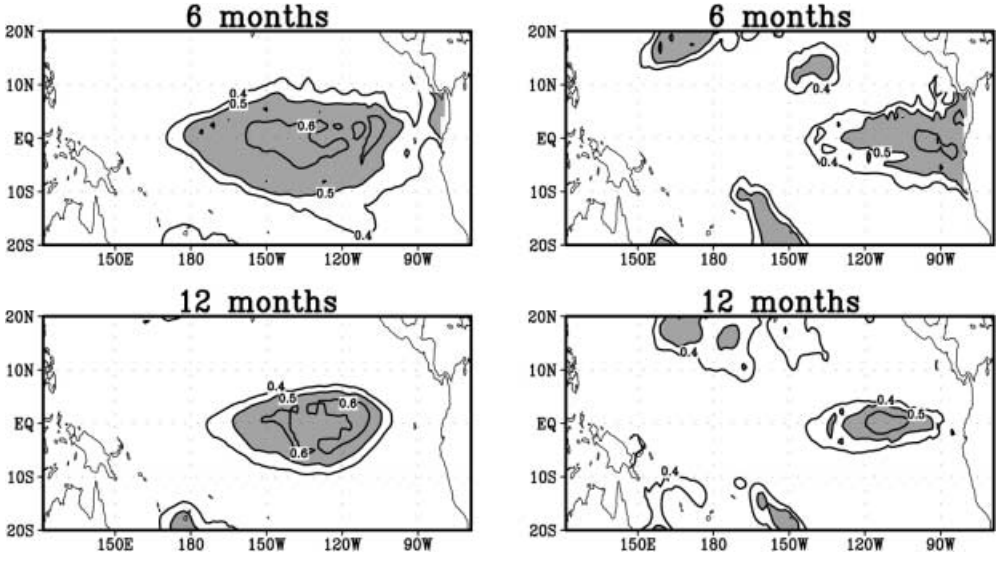

Fig. 3. Correlation skills for the predictions of SST anomalies in the tropical Pacific for the hindcast period from 1964–1990 (*left panels*), and the forecast period from 1990–1998 (*right panels*), by the LHCM. Contour interval = 0.1 and positive values over 0.5 are *shaded*

(Wallace et al. 1998); (2) anthropogenic global warming (Trenberth and Hoar 1997); (3) the interaction between tropical and extratropical oceans to produce decadal variations in the mean thermocline structure of the tropical Pacific (Gu and Philander 1997); and (4) amplification of the decadal signal through atmospheric high-frequency variability (Kirtman and Schopf 1998).

Decadal variability in the Pacific ocean also considerably affects the performances of the two coupled models. Comparing Fig. 1 with Fig. 3, we found that the difference in correlation skills between the hindcast and forecast periods is much more pronounced in the LHCM than in the NHCM. Here, the LHCM had good prediction skills in the hindcast period but suffered low skills in the 1990s like many models aforementioned. Figure 4 shows the decadal dependence of predictability in the two coupled models. The obvious decadal changes of prediction skills appear only for the LHCM. For the NHCM, except for the low skill in the 1970s which was probably associated with poor data quality and low signal-to-noise ratio (Chen et al. 1997), prediction skills did not have significant changes during the 1960s, 1980s and 1990s. In particular, in the LHCM, there is a large drop in skills from the 1980s to the 1990s, which is absent in the NHCM. We will discuss the possible cause of this difference in the next section.

Figure 5 shows the predicted Niño3 SSTA during 1980–1998 with the NHCM and the LHCM at the lead time of 6 and 12 months. As shown in Fig. 5, both models can fairly well predict the SSTA variations, and capture the ENSO variations. The common defect, as in many ENSO models (e.g., Syu and Neelin 2000; Ji et al. 2000), is the phase delay for the predicted peak time, which seems more severe in the LHCM predictions.

3.2 SLHA prediction

An important component of the coupled ocean–atmosphere system on the interannual timescale is the upper ocean heat content, which can be well characterized by SLHA variations. It is also the source of memory for the coupled system. As many studies have shown (e.g., Zebiak and Cane 1987; Rosati et al. 1997) that the fluctuations in the upper-ocean heat content (and SLHA) are both systematic and significant in the evolution of ENSO, it is of interest to examine the SLHA prediction skills.

Figures 6 and 7 show the correlation and RMSE skills of the predicted SLHA from the NHCM for the hindcast period 1980–1990 and the forecast period 1990–1998, with respect to the NCEP reanalysis product. The prediction skills share many features similar to the SSTA predicted skills. For example, the good correlation skills also mainly reside in the central and eastern Pacific and decrease toward the west and higher latitudes as in Fig. 1. However, the SLHA predictions also display some features which are absent in the SSTA predictions: (1) there exists a region of good correlation skills at the off-equatorial northern Pacific in SLHA prediction during the period 1980–1990 (Fig. 6) which is absent in the SSTA prediction; (2) except in the western Pacific, the good correlation skills in the eastern and central Pacific almost stabilize with the lead time in the SLHA predictions, in contrast with the steady decrease of correlation skills with lead time in the SSTA predictions (Fig. 1); (3) besides the high RMSE along the east coast (Fig. 7), there is another high RMSE region near the west coast in the SLHA predictions; (4) the correlation skills are higher in SLHA predictions than in SSTA predictions, especially at lead times longer than 6 months. These features are also manifested in the LHCM results (not shown).

The SLHA prediction skills also show decadal dependence, the good correlation skills occur in the equatorial central-eastern Pacific around 150°W–120°W in the 1980s, but much closer to the east coast in the 1990s (Fig. 6). The RMSE is considerably higher in the 1990s than in the 1980s (Fig. 6). The NINO3 region SLHA prediction skills during the two separate decades for various lead times (Fig. 8) reveal that the correlation skills from the LHCM show more decadal variability than those from the NHCM, similar to Fig. 4.

The predicted Niño3 SLHA during 1980–1998 from the NHCM and the LHCM at lead times of 6 and 12 months (Fig. 9) shows both models capable of predicting the Niño3 SLHA

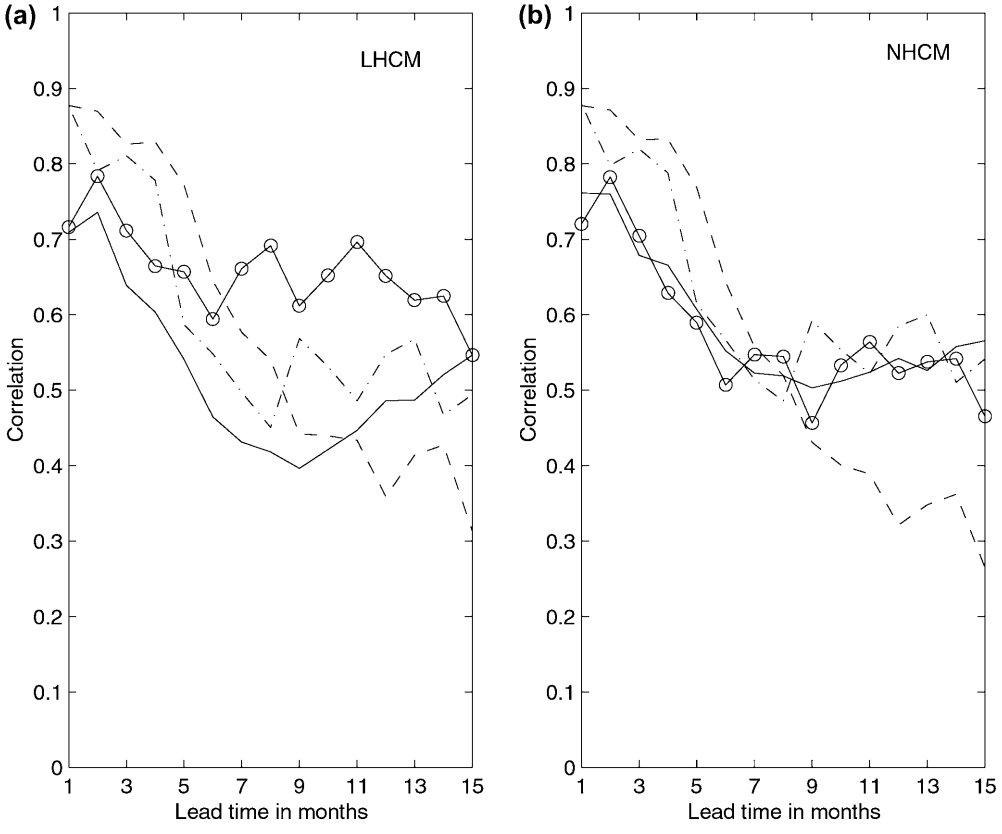

Fig. 4a,b. Correlation skills of the predicted NINO3 SSTA from A the LHCM and B the NHCM, for the 1990s (*solid*), 1980s (*circled*), 1970s (*dashed*), and the 1960s (*dot-dashed*), as a function of the lead time

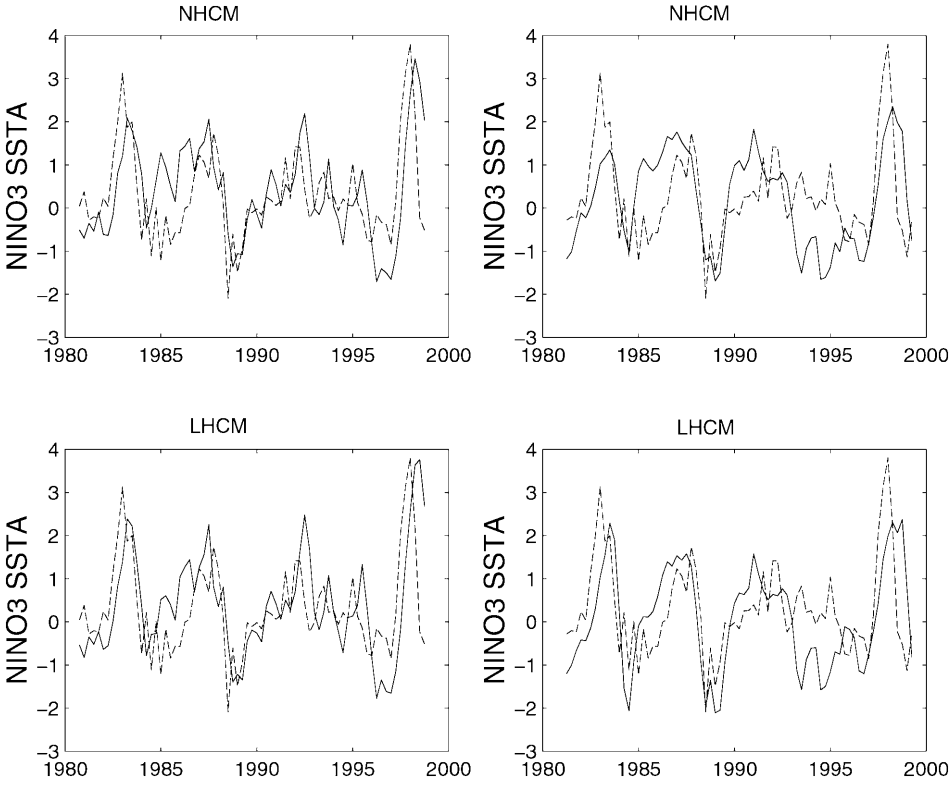

Fig. 5. Predicted NINO3 SST anomalies (°C) by the NHCM (*top panel*) and the LHCM (*bottom panel*) during 1980–1998 at 6-month (*left panels*) and 12-month (*right panels*) lead times. The *solid line* is for the predicted values and the *dashed line* for the observations

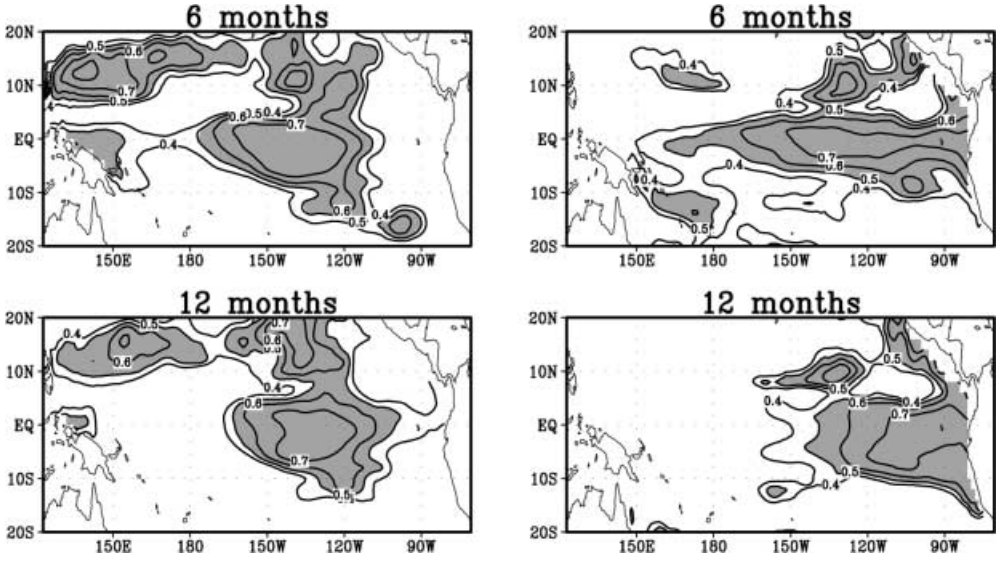

Fig. 6. Correlation skills for the predictions of SLH anomalies (with respect to the NCEP reanalysis data) for the hindcast period from 1980–1990 (*left panels*), and the forecast period from 1990–1998 (*right panels*), from the NHCM. Contour interval = 0.1 and positive values over 0.5 are *shaded*

variations, and capturing the ENSO signatures. The common defect in the SSTA predictions (Fig. 5), i.e., the phase delay in the predicted peak time, has been alleviated in the SLHA predictions (Fig. 9), indicating that the coupled models are more capable of predicting the SLHA.

In summary, both coupled models have better predicted correlation skills for the SLHA than for the SSTA, with a correlation of around 0.7 for the SLHA and 0.5 for the SSTA at a lead time of 12 months. The regions of high prediction skills shifted towards the eastern boundary in the 1990s, with the skills of the LHCM showing greater decadal variability than those of the NHCM. In the next section, we will investigate these decadal changes.

4 A possible cause for decadal dependence of ENSO predictability

Using a neural network model for nonlinear canonical correlation analysis (NLCCA, Hsieh 2000), Hsieh (2001) found that the relation between the tropical Pacific SST and the sea level pressure has become more nonlinear with time. We applied the NLCCA of Hsieh (2001) to study the relation between the first three principal components (PCs) (i.e., the EOF time coefficients) of the

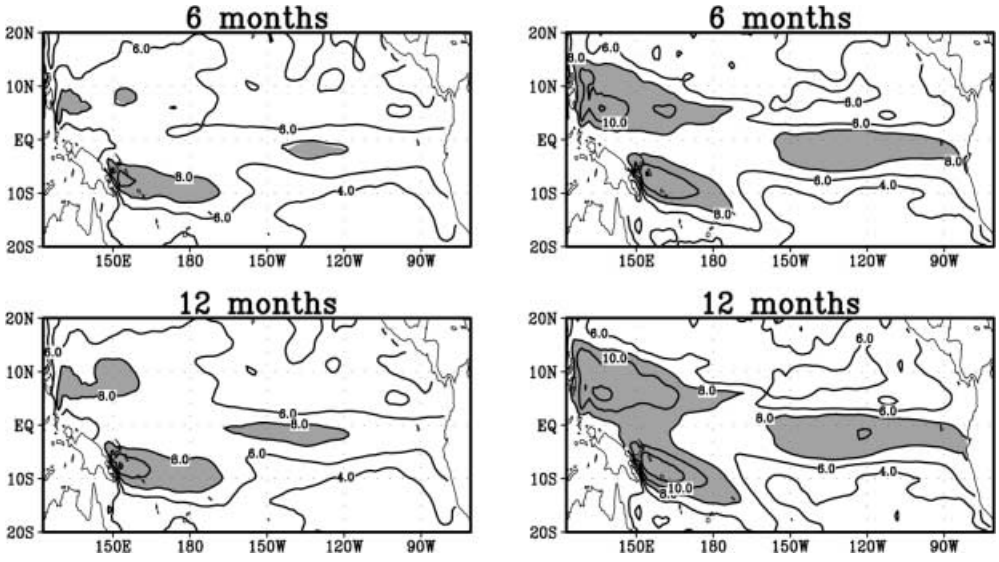

Fig. 7. RMSE skills for the predictions of SLH anomalies in tropical Pacific for the hindcast period from 1980–1990 (*left panels*), and the forecast period from 1990–1998 (*right panels*), from the NHCM. Contour interval = 2 cm and positive values over 8 cm are *shaded*

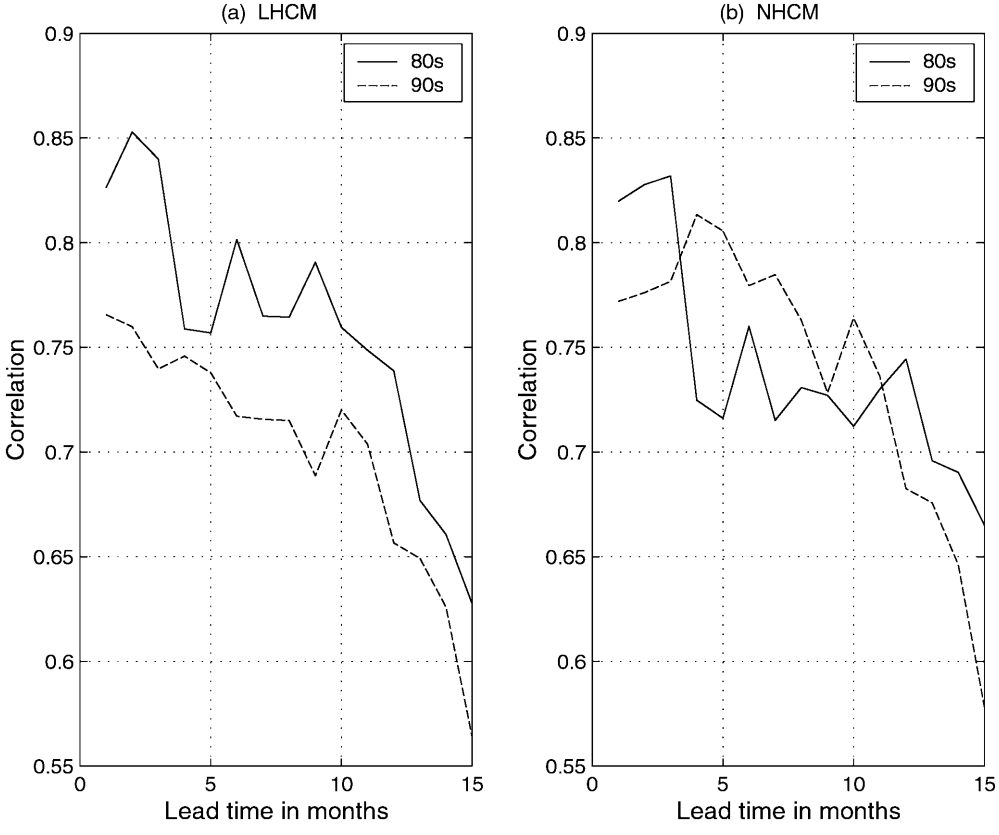

Fig. 8a,b. Predictive (correlation) skills of the NINO3 SLHA from **a** the LHCM and **b** the NHCM, for the 1980s (*solid*), and the 1990s (*dashed*), as a function of the lead time

observed zonal wind stress anomalies and the first three PCs of the observed SSTA. PC analysis (i.e., EOF analysis) was first performed for the period 1964–1999 for the zonal wind stress anomalies and the SSTA separately. The NLCCA was then applied to the PCs in the 1980s, then to the PCs in the 1990s. The first NLCCA mode for the 1980s is shown in the PC-space of the zonal wind stress anomalies and in the PC-space of the SSTA (Fig. 10). The classical CCA solutions are shown as straight lines in Fig. 10 for comparison. As a measure of the degree of nonlinearity in the relation, the ratio R between the MSE (mean square error) of the NLCCA mode to the MSE of the CCA mode can be calculated. A small R would indicate a nonlinear relation, while $R \approx 1$ would indicate an essentially linear relation. R is 0.941 for the zonal wind stress, and 0.917 for the SSTA in the 1980s. In contrast, the NLCCA mode 1 is shown in Fig. 11 for the 1990s. It is evident that the relation in the 1990s has become more nonlinear. R is 0.810 for the zonal wind stress and 0.507 for the SSTA, both

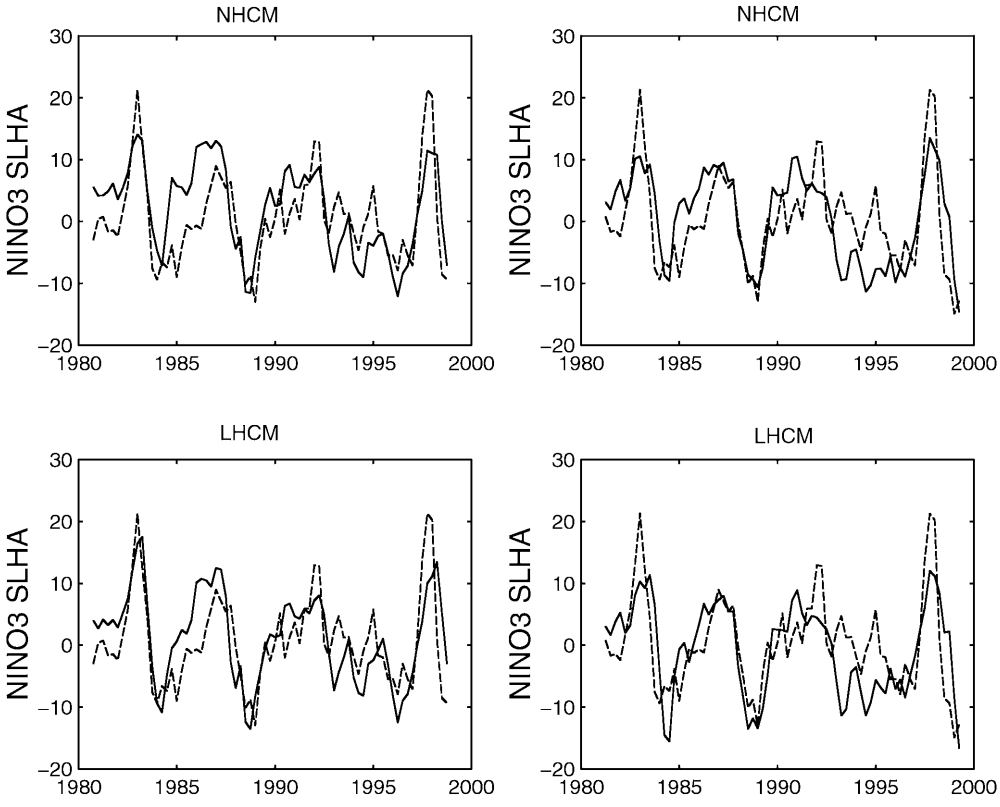

Fig. 9. Predicted NINO3 SLH anomalies (°C) by the NHCM and the LHCM during 1980–1998 at 6-month (*left panels*) and 12-month (*right panels*) lead times. The *solid line* is for the predicted values and the *dashed line* for the NCEP reanalysis SLHA

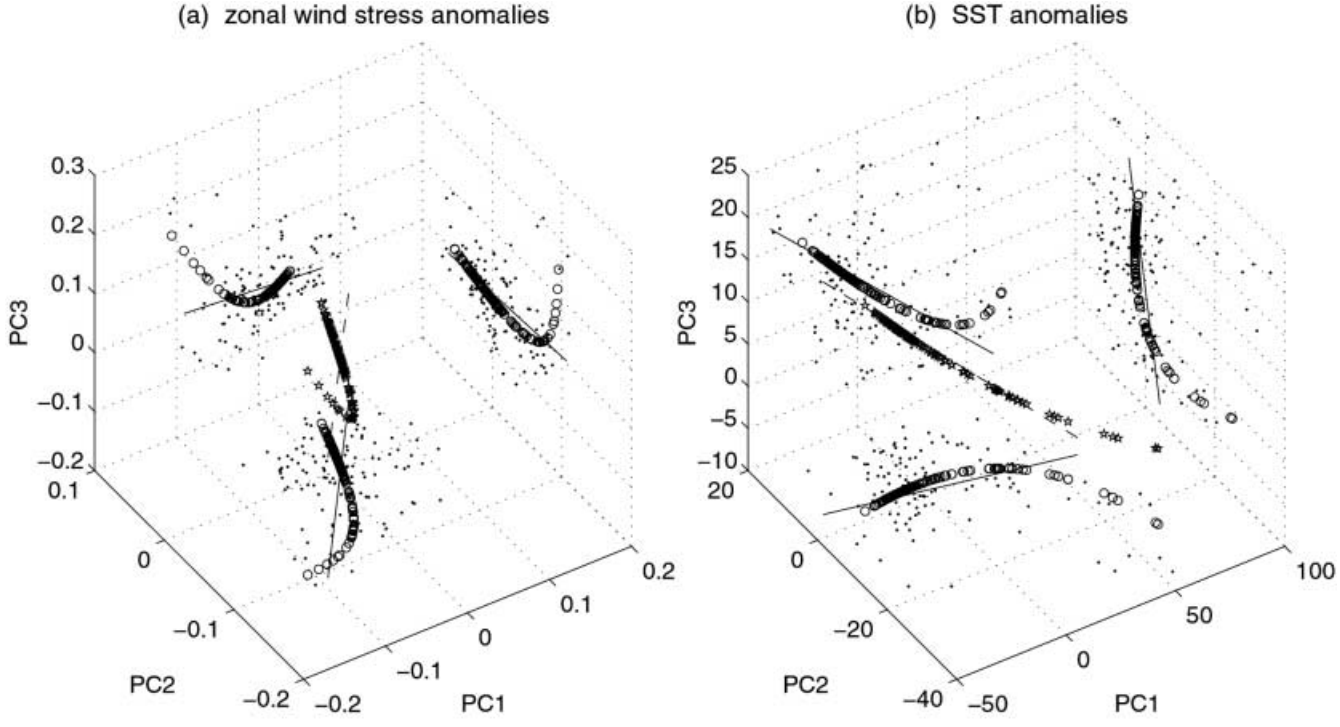

Fig. 10a,b. Nonlinear CCA (NLCCA) mode 1 for the 1980s shown in the PC (principal component) space of A the zonal wind stress anomalies and B the SST anomalies. The NLCCA analyzed the relation between the first three PCs of the zonal wind stress anomalies and the first three PCs of the SSTA. The NLCCA mode 1 is shown by the *overlapping stars*. The projections of this mode onto the PC1-PC2, PC1-PC3, PC2-PC3 planes are denoted by the *overlapping circles*, and the projected data by *dots*. For comparison, the linear CCA mode 1 is shown by the *dashed line* in the 3-D space, and by the *projected solid lines* on the 2-D planes. Following the principle of parsimony, the architecture of the NLCCA was set for minimal nonlinearity, i.e., only two hidden neurons used, and the weight penalty parameter was 0.1 in all cost functions

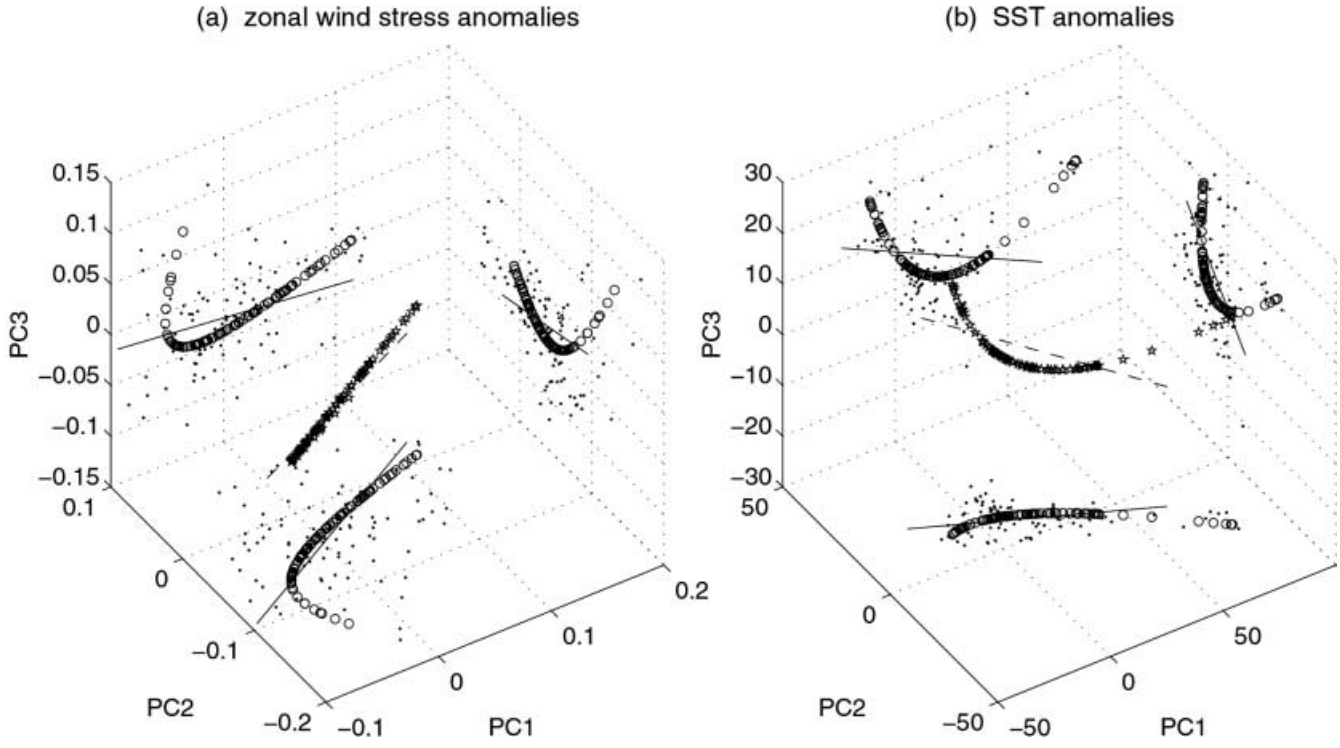

Fig. 11a,b. NLCCA mode 1 for the 1990s shown in the PC space of A the zonal wind stress anomalies and B the SST anomalies

considerably lower than the corresponding values for the 1980s.

We also plotted the NLCCA mode 1 anomaly patterns of the zonal wind stress associated with the extremes of the canonical variate u, i.e., during minimum(u) and during maximum(u) (Fig. 12), for the 1980s and for the 1990s. It is clear that during the 1980s, the pattern for min(u), i.e., La Niña, is closer to being a mirror image of the pattern for max(u), i.e., El Niño (though with weaker amplitude), than during the 1990s, as expected from the weaker nonlinearity of the 1980s. For comparison, with the CCA, the pattern for the La Niña is the mirror image of the El Niño pattern, as the CCA mode is simply a standing wave oscillation. Similarly, the NLCCA mode 1 anomaly patterns of the SST are shown in Fig. 13. During La Niña, the 1990s display a much narrower cool equatorial band than in the 1980s, rendering the La Niña pattern of the 1990s even more different from being the mirror image of the El Niño pattern, again expected from the increased nonlinearity in the 1990s.

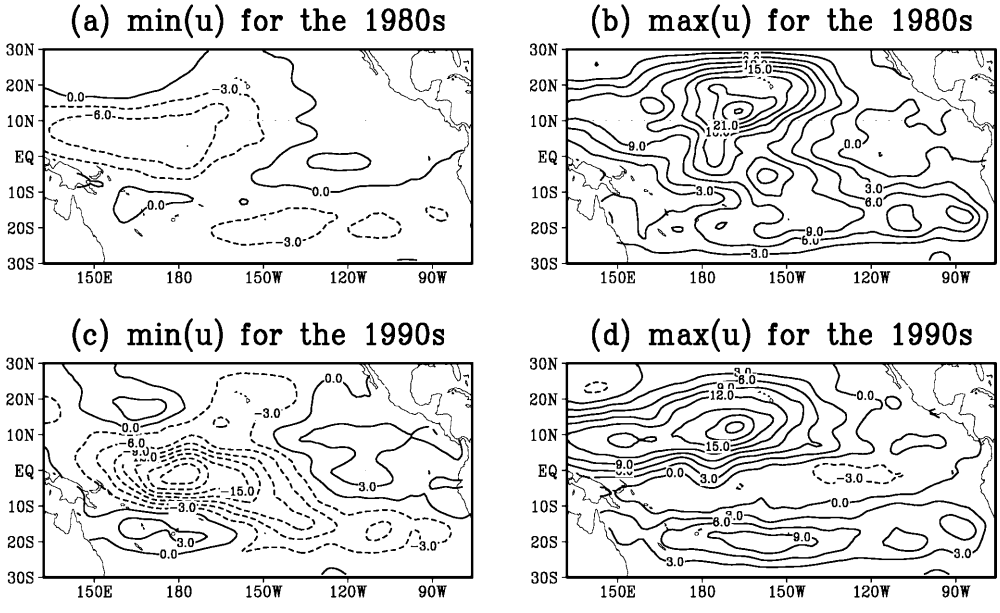

Fig. 12a–d. Zonal wind stress anomalies when the canonical variate u is minimum (*left panels*, corresponding to La Niña) and maximum (*right panels*, corresponding to El Niño). The anomalies during the 1980s are shown in **a** and **b**, and during the 1990s in **c** and **d**. The values were amplified by 100 times prior to plotting. The contour intervals are 3 N m^{-2}, with negative contours *dashed*

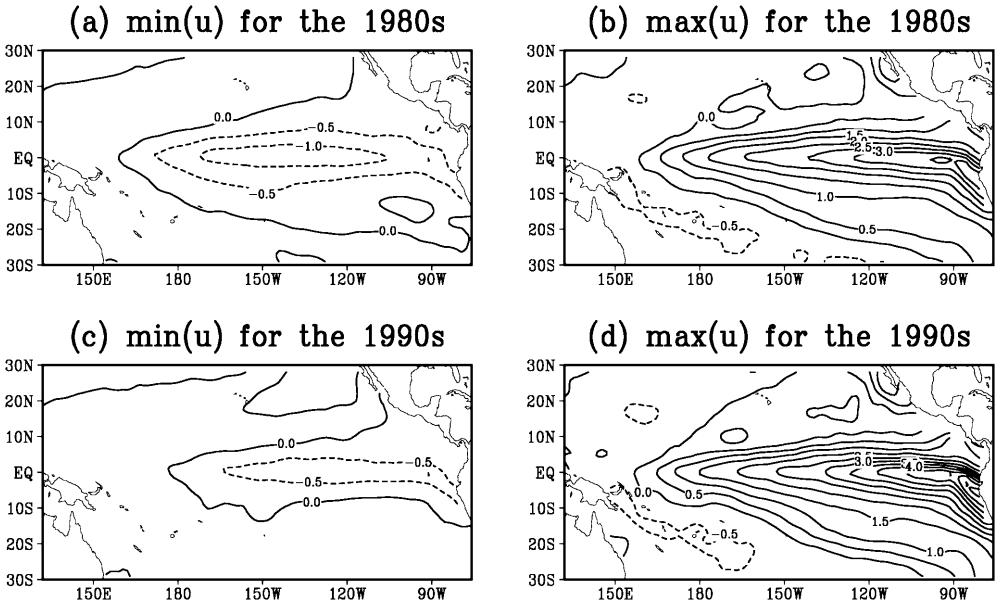

Fig. 13a–d. SST anomalies when the canonical variate u is minimum (*left panels*) and maximum (*right panels*). The anomalies during the 1980s are shown in **a** and **b**, and during the 1990s in **c** and **d**. Contour intervals are 0.5 °C

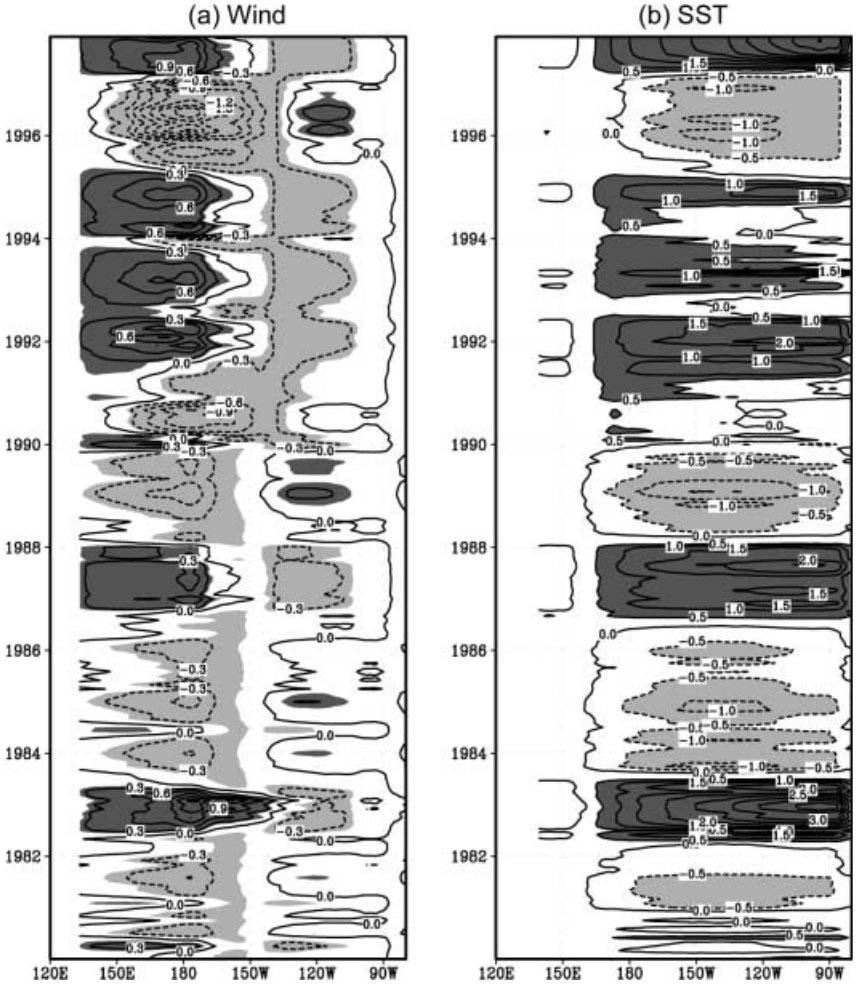

Fig. 14a, b. Time-longitude plot of the zonal wind stress anomalies (*left panel*) and SST anomalies (*right panel*) along the equator, reconstructed from the NLCCA mode 1. The contour interval is 0.3 N m^{-2} in A and 0.5 °C in B. Areas with absolute values over 0.2 N m^{-2} and over 0.5 °C are shaded in A and B respectively. The values were amplified by 10 times in A prior to plotting

Using the nonlinear technique of NLCCA, we have found that indeed the relation between the zonal wind stress and the SSTA has become more nonlinear in the 1990s than in the 1980s. The canonical correlation patterns between the wind stress anomalies and SSTA nonlinearly varied with the variations of wind stress

anomaly field. This could explain why LHCM, which did well in the 1980s, fared poorly in the 1990s, and why NHCM, which is capable of simulating the nonlinear relation between the wind stress and the surface ocean conditions, did not suffer a loss of forecast skills as the relation turned more nonlinear for the 1990s.

Wind stress and SST anomaly fields were reconstructed from the NLCCA mode 1 to illustrate the temporal evolution of the spatial patterns (Fig. 14). In the 1980s, the western Pacific was mainly controlled by the easterly anomalies, whereas in the 1990s, the westerly anomalies dominated. Correspondingly, the NLCCA mode 1 SSTA featured mainly cool anomalies in the 1980s and El Niño events in the 1990s. An interesting feature in the Fig. 14 is the asymmetry in the NLCCA mode: when the easterly anomalies prevail in the western Pacific, the maximum correlated center in the SSTA is around 150°W–120°W, but when the westerly anomalies prevail in the western Pacific, the maximum correlated center in the SSTA is shifted eastward to the eastern boundary. This seems to explain why the NHCM has good prediction skills centered around 150°W–120°W in the 1980s, but the area of high prediction skills shifted to the eastern boundary in the 1990s (Fig. 1).

5 Summary and discussion

We have examined the ENSO prediction skills in two coupled models, NHCM (which has a neural network atmosphere) and LHCM (which has a linear regression atmosphere). Both coupled models can fairly well predict the SSTA and SLHA variations of the equatorial eastern Pacific. The LHCM prediction skills display considerably more decadal variability than those of the NHCM. Both models have better predicted correlation skills for the SLHA than for the SSTA, with a correlation around 0.5 for the SSTA and 0.7 for the SLHA in the equatorial eastern Pacific up to a lead time of 1 year or so.

Compared with the earlier period (1980s), the region of high predicted skills (correlation) shifted eastward in the 1990s. This shift is probably associated with the variations of maximum correlated regions between the atmospheric anomalies (wind stress anomalies) and ocean anomalies (SSTA) in the two decades. In the 1980s, the easterly wind prevailed over the equatorial western Pacific, and according to the NLCCA mode 1, the correlated region for the SSTA was centered in the equatorial Pacific around 150°W–120°W. In the 1990s, the westerly wind prevailed over the equatorial western Pacific, and the correlated region for the SSTA shifted to the eastern boundary. It has been found that the ENSO signals in the 1990s differ notably from conventional ENSO characteristics (Kleeman et al. 1996). For the El Niño episodes in the 1990s, the warming generally first occurred in the central equatorial Pacific, then propagated into the eastern Pacific, whereas before the 1990s, ENSO signatures were generally characterized by the westward propagation of warming from the anomalous regions along the South American coast into the central equatorial Pacific. Kleeman et al. (1996) noted that the 1990s anomaly is associated with non-equatorial physical processes, quite unlike the usual ENSO which is thought to have strong connections with equatorial physics.

The main difference in forecast skills between the NHCM and the LHCM occurred in the 1990s, where the NHCM had better skills. A nonlinear CCA (NLCCA) analysis of the zonal wind stress anomalies and the SSTA shows that their relation was indeed more nonlinear in the 1990s than in the 1980s, which would give the NHCM an advantage over the LHCM in the 1990s, as the LHCM does not have the capability of simulating nonlinear relations between the wind stress and the surface ocean conditions.

Acknowledgements We would like to thank two anonymous reviewers for their valuable comments, and Prof. K. Haines, Prof. D. L. T Anderson and Dr. M. A. Balmaseda for providing their ocean model used in our hybrid coupled models. This work has benefited from discussions with Magdalena Alonso Balmaseda, Keith Haines, Benyang Tang, Yun Fang and Zhaoyong Guang. This work was supported by research and strategic grants to W. Hsieh from the Natural Sciences and Engineering Research Council of Canada.

References

Balmaseda MA, Anderson DLT, Davey MK (1994) ENSO prediction using a dynamical ocean model coupled to statistical atmospheres. Tellus46(A) 4: 497–511

Balmaseda MA, Davey MK, Anderson DLT (1995) Decadal and seasonal dependence of ENSO prediction skill. J Clim 8: 2705–2715

Barnett TP, Latif M, Graham NE, Flügel M, Pazan S, White W (1993) ENSO and ENSO related predictability. Part1: prediction of equatorial sea surface temperature with a hybrid coupled ocean–atmosphere model. J Clim 6: 1545–1566

Blanke B, Neelin JD, Gutzler D (1997) Estimating the effect of stochastic wind stress forcing on ENSO irregularity. J Clim 10: 1473–1486

Chang P, Ji L, Li H, Flügel M (1996) Chaotic dynamics versus stochastic processes in El Niño-Southern Oscillation in coupled ocean–atmosphere models. Physica D 98: 301–320

Chen D, Zebiak SE, Cane MA, Busalacchi AJ (1997) Initialization and predictability of a coupled ENSO forecast model. Mon Weather Rev 125: 773–788

Flügel M, Chang P (1998) Does the predictability of ENSO depend on the seasonal cycle? J Atmos Sci 55: 3230–3243

Goldenberg B, O'Brien JJ (1981) Time and space variability of tropical Pacific wind stress. Mon Weather Rev 109: 1190–1207

Gu D, Philander SGH (1997) Interdecadal climate fluctuation that depend on exchanges between the tropics and the extra-tropics. Science 275: 805–807

Hsieh WW (2000) Nonlinear canonical correlation analysis by neural networks. Neural Networks 13: 1095–1105

Hsieh WW (2001) Nonlinear canonical correlation analysis of the tropical Pacific climate variability using a neural network approach. J Clim 14: 2528–2539

Hsieh WW, Tang B (1998) Applying neural network models to prediction and analysis in meteorology and oceanography. Bull Am Meteorol Soc 79: 1855–1870

Ji M, Leetmaa A, Kousky VE (1996) Coupled model prediction of ENSO during the 1980s and 1990s at the National Centers for Environmental Prediction. J Clim 9: 3105–3120

Kang I, Kug J (2000) An El Niño prediction system using an intermediate ocean and a statistical atmosphere. Geophys Res Lett 27: 1167–1170

Kleeman R, Colman RA, Smith NR, Power SB (1996) A recent change in the mean state of the Pacific basin climate: observational evidence and atmospheric and oceanic responses. J Geophys Res 101: 20,483–20,499

Kirtman B, Schopf PS (1998) Decadal variability in ENSO predictability and prediction. J Clim 11: 2804–2822

Latif M, Kleeman R, Eckert C (1997) Greenhouse warming, decadal variability or ENSO? An attempt to understand the anomalous 1990s. J Clim 10: 2221–2239

Latif M, Anderson DLT, Barnett T, Cane M, Kleeman R, Leetmaa A, O'Brien JJ, Rosati A, Schneider E (1998) A review of the predictability and prediction of ENSO. J Geophys Res 103: 14,375–14,393

Palmer TN, Anderson DLT (1994) The prospects for seasonal forecasting – A review paper. Q J R Meteorol Soc 7: 755–793

Rosati A, Miyakoda K, Gudgel R (1997) The impact of ocean initial conditions on ENSO forecasting with a couple model. Mon Weather Rev 125: 754–772

Syu H-H, Neelin JD (2000) ENSO in a hybrid coupled model. Part II: prediction with piggyback data assimilation. Clim Dyn 16: 35–48

Tang B, Hsieh WW, Monahan AH, Tangang FT (2000) Seasonal predictions of sea surface temperatures in the tropical Pacific – comparing neural networks and canonical correlation analysis. J Clim 13: 287–293

Tang Y, Hsieh WW, Tang B, Haines K (2001) A neural network atmospheric model for hybrid coupled modeling. Clim Dyn 17: 445–455

Tang Y (2002) Hybrid coupled models of the tropical Pacific, Part I. Interannual variability. Clim Dyn (in press). DOI 10.1007/s00382-002-0230-3

Trenberth K, Hoar TJ (1997) El Niño and climate change. Geophys Res Lett 24: 3057–3060

Wallace JM, Rasmusson E, Mitchell T, Kousky V, Sarachik E, von Storch H (1998) On the structure and evolution of ENSO-related climate variability in the tropical Pacific: lessons from TOGA. J Geophys Res 103: 14,241–14,259

Wang B (1995) Interdecadal changes in El Niño onset in the last four decades. J Clim 8: 267–285

Zebiak SE, Cane MA (1987) A model El Niño-Southern Oscillation. Mon Weather Rev 115: 2262–2278

Zhang Y, Wallace JM, Battisti DS (1997) ENSO-like interdecadal variability: 1900–93. J Clim 10: 1004–1020